JOURNAL OF THE KOREAN ASTRONOMICAL SOCIETY
40: 67 ~ 82, 2007

Hα SPECTRAL PROPERTIES OF VELOCITY THREADS CONSTITUTING A QUIESCENT SOLAR FILAMENT

JONGCHUL CHAE[1], HYUNG-MIN PARK[2] AND YOUNG-DEUK PARK[2]
[1]Astronomy Program & FPRD, Department of Physics and Astronomy, Seoul National University, Seoul 151-747, Korea
e-mail: chae@astro.snu.ac.kr
[2] Korea Astronomy and Space Science Institute, Whaamdong, Yooseong, Daejeon, 305-348, Korea
(Received September 17, 2007; Accepted September 21, 2007)

ABSTRACT

The basic building block of solar filaments/prominences is thin threads of cool plasma. We have studied the spectral properties of velocity threads, clusters of thinner density threads moving together, by analyzing a sequence of Hα images of a quiescent filament. The images were taken at Big Bear Solar Observatory with the Lyot filter being successively tuned to wavelengths of -0.6, -0.3, 0.0, +0.3, and +0.6 Å from the centerline. The spectra of contrast constructed from the image data at each spatial point were analyzed using cloud models with a single velocity component, or three velocity components. As a result, we have identified a couple of velocity threads that are characterized by a narrow Doppler width ($\Delta\lambda_D = 0.27$ Å), a moderate value of optical thickness at the Hα absorption peak ($\tau_0 = 0.3$), and a spatial width (FWHM) of about 1″. It has also been inferred that there exist 4–6 velocity threads along the line of sight at each spatial resolution element inside the filament. In about half of the threads, matter moves fast with a line-of-sight speed of 15 ± 3 km s^{-1}, but in the other half it is either at rest or slowly moving with a line-of-sight velocity of 0 ± 3 km s^{-1}. It is found that a statistical balance approximately holds between the numbers of blue-shifted threads and red-shifted threads, and any imbalance between the two numbers is responsible for the non-zero line-of-sight velocity determined using a single-component model fit. Our results support the existence not only of high speed counter-streaming flows, but also of a significant amount of cool matter either being at rest or moving slowly inside the filament.

Key words : Sun: atmospheric motions — Sun: chromosphere — Sun: filaments — Sun: magnetic fields — Sun: prominences

I. INTRODUCTION

Observations of prominences outside the solar limb (Engvold 1976; Engvold et al. 1989; Zirker & Koutchmy 1990, 1991; Mein & Mein 1991) and filaments on the solar disk (Simon et al. 1986; Mein et al. 1994; Lin et al. 2005) have supported the view that the basic building block of prominences/filaments is threads that are too thin to be spatially resolved in most observations. Each spatial resolution element of observations carries mixed information on a number of threads that exist along the line of sight inside the square area on the plane of the sky. Statistical modelling has often been used to infer the number of threads and mean properties of threads. Limb observations have indicated that the number of threads in the resolution element range from a few (Engvold et al. 1989) to 20 (Zirker & Koutchmy 1990) while disk observations yielded smaller values for most spatial elements (Mein et al. 1994).

Mein & Mein (1991) emphasized the importance of distinguishing between the concepts of 'velocity threads' and 'density threads'. A velocity thread may be defined as a thread inside which bulk motion slowly varies with position, whereas a density thread is one inside which temperature and density vary slowly. They suggested that velocity threads consist of bundles of cool density threads driven by similar motions. As a consequence, the characteristic scale L_V of the velocity field should be larger than that of the density or temperature, L_T. These two scales should be smaller than that of the magnetic field L_B, resulting in the inequalities $L_T < L_V < L_B$, as summarized by Mein (1994). The width of velocity threads may be of the order of 1″ (Mein & Mein 1991) while that of density threads may be much smaller. It may be velocity threads that have been statistically modelled in previous studies (Engvold et al. 1989; Zirker et al. 1990, 1991; Mein & Mein 1991; Mein et al. 1994). Only the highest spatial resolution observations such as those done by the 1 m Swedish Solar Telescope (Lin et al. 2005) succeeded in spatially resolving density threads in filaments. From these observations it has been found that the FWHM widths of density threads range from 0.2 to 0.6 arc seconds, with an average of about 0.3 arc seconds.

During the last decade there has been increasing evidence from Hα observations (Zirker et al. 1998; Chae et al. 2000; Lin et al. 2003, 2005) and UV/EUV

Corresponding Author: J. Chae

observations (Wang 1999; Chae 2003; Kucera et al. 2003; Kucera & Landi 2006) that plasmas in prominences/filaments often move at significant speeds along threads. It appears that plasma in a velocity thread moves independently of that in neighboring threads, resulting in the velocity pattern of counter-streaming (Zirker et al. 1998). Since the threads are the building blocks of filaments, and motion characterizes individual threads, it is essential to reveal the physical nature of the motion in threads for the study of filament fine structure.

Zirker et al.(1998) proposed that the existence of such fast moving plasma may negate the need for dip-like magnetic structures that have been thought to sustain cool plasma high in the corona against gravity. Thermal instability has been considered as the physical origin of such high-speed motion (Karpen et al. 2006 and references therein). In such models, magnetic dips are not an essential ingredient for supporting cool plasma in prominences/filaments. If this kind of idea is to be effective, all the threads should be dynamic, filled with fast-moving plasma. This theoretical expectation needs to be verified observationally.

Basically there are two different ways to infer the motion in threads from observations. One is to make use of spectral information in data to infer the line-of-sight velocity. The other is to use a time series of images to infer the transverse velocity in the plane of sky. In principle, these methods, when combined, can yield the velocity vectors that are crucial in interpreting the geometry of the motion. Such an attempt was made by Lin et al. (2003). They used the technique of stack plots of slices and successfully inferred the transverse velocities. The line-of-sight velocities they deduced, however, were seriously underestimated, even if they may have had the correct signs, because the Doppler signal they used is contributed to not only by the filament, but also by the underlying chromosphere, as discussed in our previous work (Chae et al. 2006, hereafter Paper I). This kind of limitation mainly arises from the shortage of spectral information, since only three wavelengths were used to determine the Doppler shift in the work of Lin et al. (2003).

In Paper I, we showed that the inclusion of two more wavelengths significantly increases the accuracy of the line-of-sight velocity as well as the number of physical parameters to be obtained. It was also described in Paper I how to reduce the spectral profiles of intensity contrast from observations, and it was shown that the profiles are usually well fitted by the cloud model. Maps of optical thickness, line-of-sight velocity, and absorption width obtained from this kind of data may be useful for inferring the physical parameters and internal dynamics in filaments.

The objective of the present paper is to infer the spectral properties of the velocity threads in a filament. We use the same set of data as was used in Paper I. Specifically we will identify a couple of velocity threads and determine the properties of a typical velocity thread. We will then apply the single velocity component cloud model fit to the data in the way described in Paper I. On top of this, we will extend the method of the cloud model to incorporate two velocity components, three velocity components, and more. Important results will be obtained from three-component cloud models.

II. OBSERVATIONS

Our Hα observations were carried out from 15:45 UT to 24:00 UT on 2004 August 3 at Big Bear Solar Observatory. The filament we observed was located on the northern hemisphere of the Sun (X=-400″, Y=+240″, N15, E26, $\cos\theta = 0.87$), inside a filament channel associated with an old active region. This filament has two well-defined barbs. The magnetic environment of these barbs was studied by Chae et al. (2005). In this study, we focus on the threads that constitute one of these barbs as well as the filament body (spine).

Figure 1 shows several sample images of the filament of our interest taken during the observation period of about 5 hours. This filament is associated with an old active region, so it may be classified as an intermediate-type filament. Like other filaments, this filament has two parts: a peninsula-like extrusion called a barb and the long axis of the filament, called a spine. The spine is slightly curved like a bow. The barb is right-bearing so the filament is a dextral filament. During our period of observation, the large-scale morphology of the filament did not change much, but the fine scale structures as represented by threads underwent ceaseless changes.

The observations were performed using a 10-inch refractor equipped with a Zeiss Hα birefringent filter of 0.25 Å bandwidth, and a fast 1024×1024 camera (DALSTASR 1M30P) made by Dalsa Corporation. One pixel of the camera corresponds to 0.375″ or 270 km on the Sun. The filter was successively tuned to the five wavelengths at Hα-0.6, -0.3, 0.0, +0.3, +0.6 Å on the basis of a computer control. The exposure time was taken to be 60 ms and the corresponding frame rate was found to be 16 fps. The technique of frame selection was applied and only the best image among 30 frames was saved at each wavelength. It took 15 s to finish one scan of five wavelengths and 4 s to resume the next scan. As a result of the observing run, we obtained a total of 7308 images that day, but in the present work we analyze only a small fraction of these data for our study.

Data processing was described in detail in Paper I. The final outcome of the data processing is contrast data defined by

$$C_\lambda^{\rm obs}(x,y) = \frac{I_\lambda^{\rm obs}(x,y) - I_\lambda^{\rm ref}}{I_\lambda^{\rm ref}} \qquad (1)$$

for $\lambda = -0.6, -0.3, 0., +0.3, +0.6$ Å from the center of the $I_\lambda^{\rm ref}$ profile. Here $I_\lambda^{\rm obs}(x,y)$ is the observed intensity

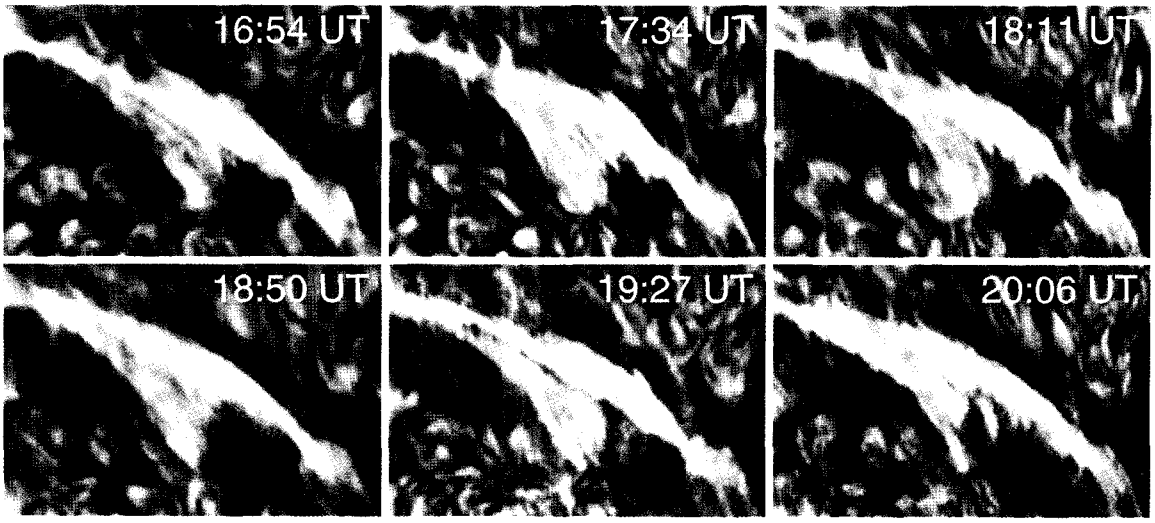

Fig. 1.— Some of true color Hα images taken at different times. Red color represents the absorption at +0.6 Å, green at 0.0 Å, and blue at -0.6 Å. The field of view is 90″ by 60″.

at an arbitrary point (x, y), and $I_\lambda^{\rm ref}$ is the intensity of the reference atmosphere below the filament, which is practically defined as the average of observed intensity over the featureless regions near the filament.

III. DATA ANALYSIS

Our data analysis is based on the widely used theory of radiative transfer for a cloud-like absorbing structure, called the cloud model, in which the theoretical contrast $C_\lambda^{\rm model}$ between the intensity emergent out from the structure $I_\lambda^{\rm out}$ and the intensity incident into it $I_\lambda^{\rm in}$ is expressed like

$$C_\lambda^{\rm model} \equiv \frac{I_\lambda^{\rm out} - I_\lambda^{\rm in}}{I_\lambda^{\rm in}} = \left(\frac{S}{I_c}\frac{I_c}{I_\lambda^{\rm in}} - 1\right)(1 - \exp(-\tau_\lambda)) \ . \tag{2}$$

The normalized Hα intensity profile $I_\lambda^{\rm in}/I_c$ is set to that at the disk center given by Wallace et al. (1998). Note that S/I_c is assumed to be independent of wavelength and also of position inside the absorbing structure.

The goodness of fit of the model at a spatial point is measured by

$$\chi^2 = \frac{1}{N_f}\sum_\lambda \frac{1}{\sigma^2}(C_\lambda^{\rm obs} - C_\lambda^{\rm model})^2 , \tag{3}$$

where N_f is the degree of freedom that is equal to the number of data points less the number of free parameters. In Paper I, we have estimated that $\sigma < 0.015$. For the present study, we choose $\sigma = 0.01$.

If the spectral information in the contrast data is not abundant enough, it may be difficult to uniquely determine all of these parameters from the data. This is the case in our data where there are only five spectral points. Therefore we have added two zero contrasts at the wavelengths $\lambda = \pm 1.5$ Å to increase the number of data points to seven. This is a reasonable approach for quiescent filaments.

An intrinsic difficulty in the analysis of filament observations is the contamination in the spectral data by the line-of-sight overlapping of highly dynamic chromospheric structures such as mottles and fibrils. The contamination makes the contrast profile too complex to allow a meaningful spectral analysis. A fortunate thing is that it is possible to discern the area of serious contamination since mottles and fibrils are prominent in the off-band wavelengths while filaments are prominent on the centerline (see Figure 1). We find from the figure that the upper-left part of the filament is subject to such contamination. In other areas, the effect of contamination is negligible.

We suppose each cloud-like absorbing structure consists of a finite number of velocity threads that are located along the line of sight, and each velocity thread has its own optical thickness whose wavelength dependence follows a Gaussian distribution.

(a) Single velocity component model

The traditional version of the cloud model adopts a single Gaussian function for the optical thickness

$$\tau_\lambda = \tau_0 \exp\left[-\left(\frac{\lambda - \lambda_0}{\Delta\lambda_D}\right)^2\right] . \tag{4}$$

The single velocity component model has four free parameters to be determined: S/I_c, τ_0, λ_0, $\Delta\lambda_D$. This model is simple and good enough for the investigation of individual threads, when only one thread lies along the line of sight. However, usually there is more than one thread along the line of sight, so the parameters obtained from single-component model fits may represent

those not of individual threads, but of their combined effects. Paper I presents some details on the single-component cloud model fit.

The line-of-sight velocity of the thread is given by $v_0 = 45\lambda_0$ km s^{-1}, when λ_0 is given in units of Å. Recall both λ and λ_0 are measured from the center of the reference Hα line profile that has been taken from the average atmosphere of featureless regions surrounding the filament.

(b) Two velocity-component model

The next simplest model is the two velocity-component model

$$\tau_\lambda = \tau_r \exp\left[-\left(\frac{\lambda-\lambda_r}{\Delta\lambda_D}\right)^2\right] + \tau_b \exp\left[-\left(\frac{\lambda-\lambda_b}{\Delta\lambda_D}\right)^2\right] \quad (5)$$

with four free parameters to be determined: τ_r, λ_r, τ_b, λ_b. The parameter S/I_c is set to the value obtained from the single-component model, and the parameter $\Delta\lambda_D$ is set to 0.27 Å, the Doppler width of resolved threads. This model is suited for describing the line-of-sight overlapping of two threads moving in opposite directions.

(c) Three velocity-component model

The three velocity-component model of the form

$$\begin{aligned}\tau_\lambda &= \tau_r \exp\left[-\left(\frac{\lambda-\lambda_r}{\Delta\lambda_D}\right)^2\right] + \tau_s \exp\left[-\left(\frac{\lambda}{\Delta\lambda_D}\right)^2\right] \\ &+ \tau_b \exp\left[-\left(\frac{\lambda-\lambda_b}{\Delta\lambda_D}\right)^2\right] \quad (6)\end{aligned}$$

is the simplest model that can represent the stationary, blue-shifted, and red-shifted components. This model has five free parameters to be determined: τ_r, λ_r, τ_s, τ_b, λ_b. Note that the parameters S/I_c and $\Delta\lambda_D$ are set to constant values as described above. We further reduce the number of degrees of freedom in the free parameters to be determined, by applying the constrained fitting method described in Paper I and Chae et al. (1998). Specifically we constrain λ_r, λ_b to be around the prescribed values 0.36 Å and -0.36Å, respectively, within a standard deviation of 0.20 Å from these values. The specific value of 0.36 Å was chosen to ensure the best overall goodness of fit as measured by the value of $\langle\chi^2\rangle$ averaged over all the points inside the filament.

(d) Multi velocity-component Model

An ideal model for the study of filament threads is a multi velocity-component model

$$\tau_\lambda = \sum_{i=1}^{N} \tau_i \exp\left[-\left(\frac{\lambda-\lambda_i}{\Delta\lambda_D}\right)^2\right] \quad (7)$$

TABLE 1.
PARAMETERS: THE SINGLE-COMPONENT CLOUD MODEL PARAMETERS OF VELOCITY THREAD 1.

PARAMETER	VALUE
τ_0	0.31
$\Delta\lambda_D$	0.27 Å
$\tau_0\Delta\lambda_D$	0.084 Å
WIDTH	$\sim 1''$

where every thread is considered as a velocity component. In this model, the number of threads N itself is treated as a free parameter, so that the model has $2N+1$ free parameters to be determined: N, τ_i, λ_i ($i = 1, 2, ..., N$). As in the case of three-component model, the parameter S/I_c is fixed to the value determined from the single-component fit, and the parameter $\Delta\lambda_D$ is set to the Doppler width of resolved threads.

As shall be shown later in this paper, the number of threads N is usually greater than three, so that the number of free parameters turns out to be bigger than seven. Our data have too few spectral points for this model. Therefore we cannot apply this model to our data, and our analysis is confined to the single-component model, two-component model, and three-component model.

IV. EXAMPLES OF CLOUD MODEL FITTINGS

To illustrate the results of model fitting, we study in detail four contrast profiles, representing two resolved threads, and two unresolved absorbing structures inside the barb and the spine, respectively. Figure 2 show the locations where these profiles were taken.

(a) Velocity Thread 1

The cross ($\times$) symbol in Figure 2 marks a point on a velocity thread. This red-shifted velocity thread is clearly discernable in the color image as well as the monochromatic images taken at wavelengths +0.3, +0.6 Å. The spatial location of the point was carefully chosen so that the line-of-sight overlapping of other structures is negligible. We have examined the spatial profile of contrast across these threads at +0.6 Å and found that its FWHM is about 1.6 ″. If the observational blurring (>1″) is taken into account, the true width may be estimated to be smaller than 1.2″.

It is found from Figure 3 that the contrast profile of this velocity thread is satisfactorily fitted by the single component model ($\chi^2 = 0.27$). The parameters obtained from the fit, together with the morphology shown in Figure 2 support the view that the absorbing structure is very likely to represent a resolved velocity thread. Most of all, the value of $\Delta\lambda_D$ determined from the fit, 0.27 Å, is small enough to be accounted for by a choice of the typical values of temperature ($T = 8000$)

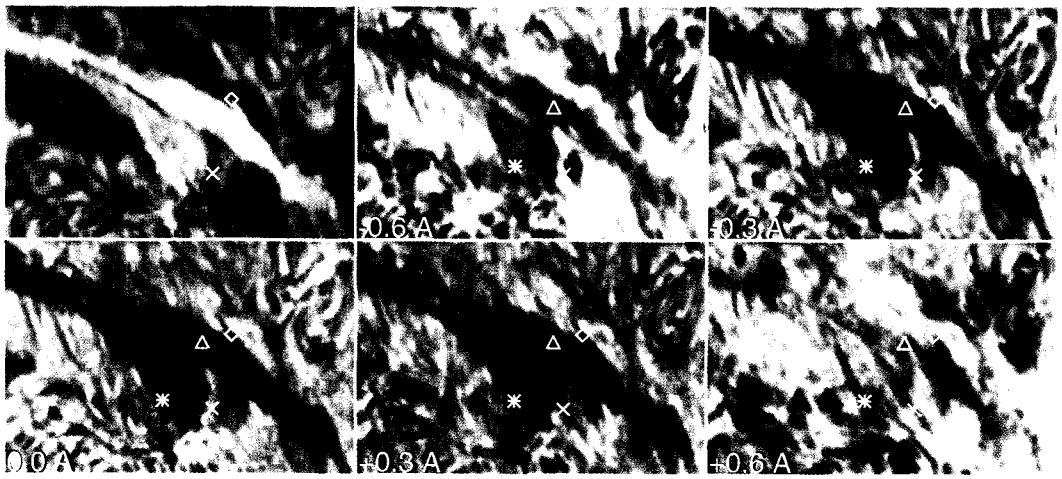

Fig. 2.— True color Hα image and gray-scale images taken at five different wavelengths. The symbols refer to the locations where sample contrast profiles were taken (two for velocity threads, one for the barb, and one for the spine).

and micro-turbulence ($\xi = 5$ km s^{-1}), leaving no room for the excess broadening due to the line-of-sight superposition of different bulk motions. It is thus consistent with the uniformity of bulk motions inside the spatial resolution element, the condition required for a velocity thread. Secondly, the optical thickness obtained from the single-component fit $\tau_0 = 0.31$ is moderately small. As we shall see later, the average optical thickness inside the filament is significantly larger than this value.

The values of the other parameters determined from the single-component fit are $S/I_c = 0.11$, and $\lambda_0 = 0.32$ Å. From the latter value we see that the thread is moving away from us at a speed of $v_0 = 14.6$ km s^{-1} along the line of sight. The parameters of this velocity thread are summarized in Table (a). It has to be recalled that the amount of cool material is proportional not to τ_0, but to $\tau_0 \Delta\lambda_D$.

Figure 3 also presents the results of a two-component fit and a three-component fit, but the results are basically the same as that of the single-component fit.

(b) Velocity Thread 2

Figure 4 presents another example of an absorbing structure at the location marked by the ◇ symbol in Figure 2. This structure looks like a resolved velocity thread, and the contrast profile is well fitted by the single-component model. From this fit we have obtained $S/I_c = 0.11$, the same value as above. However the Doppler width obtained from the fit has a value of 0.32 Å, higher than the previous value of 0.27 Å. This suggests that the contrast profile in fact represents more than one thread along the line of sight. To spectrally resolve the threads, we have applied a two velocity-component fit and a three velocity-component fit (with $\Delta\lambda_D = 0.27$ Å) to the data, respectively. Encouragingly these two model fits yielded approximately the same result, namely that the contrast profile is well decomposed into two velocity components. From the two velocity-component fit, we find the red-shifted component has an optical thickness of 0.32, and the stationary component has an optical thickness of 0.35. These values are a little bigger than, but are not much different from the value 0.31, the optical thickness of velocity thread 1. This suggests that velocity threads may have similar values for optical thickness as well as for absorption width.

(c) Barb

The $*$ symbol in Figure 2 locates a point inside the barb. It apparently refers to a red thread in the color image, but its spectral profile of contrast given in Figure 5 suggests that there may be more than one velocity thread along the line of sight at the point. The single-component model produces a reasonably good fit ($\chi^2 = 0.46$), but the Doppler width ($\Delta\lambda_D = 0.49$ Å) is too big for a single thread. The red-shifted velocity of $v_0 = 2.6$ km s^{-1} obtained from the single-component fit is quite low, but may be understood as an average velocity over the spatial resolution element.

The two component model fit is too poor ($\chi^2 = 24$) to yield any physically meaningful parameters. The failure of the fitting is related to the fixed parameter $\Delta\lambda_D = 0.27$ Å. We found that a choice 0.36 Å or higher would lead to a satisfactory fit ($\chi^2 < 1$), but the Doppler width is too big for resolved threads. Therefore, we conclude a two-component model is not suited for this contrast profile.

The three-component model with the fixed parameter $\Delta\lambda_D = 0.27$ Å, fits the contrast data extremely well, with $\chi^2 = 0.01$. This success of the three-component model together with the failure of the two-component model implies that the existence of a stationary component is crucial for explaining the contrast data.

The three component fit produced $v_r = +16.9$

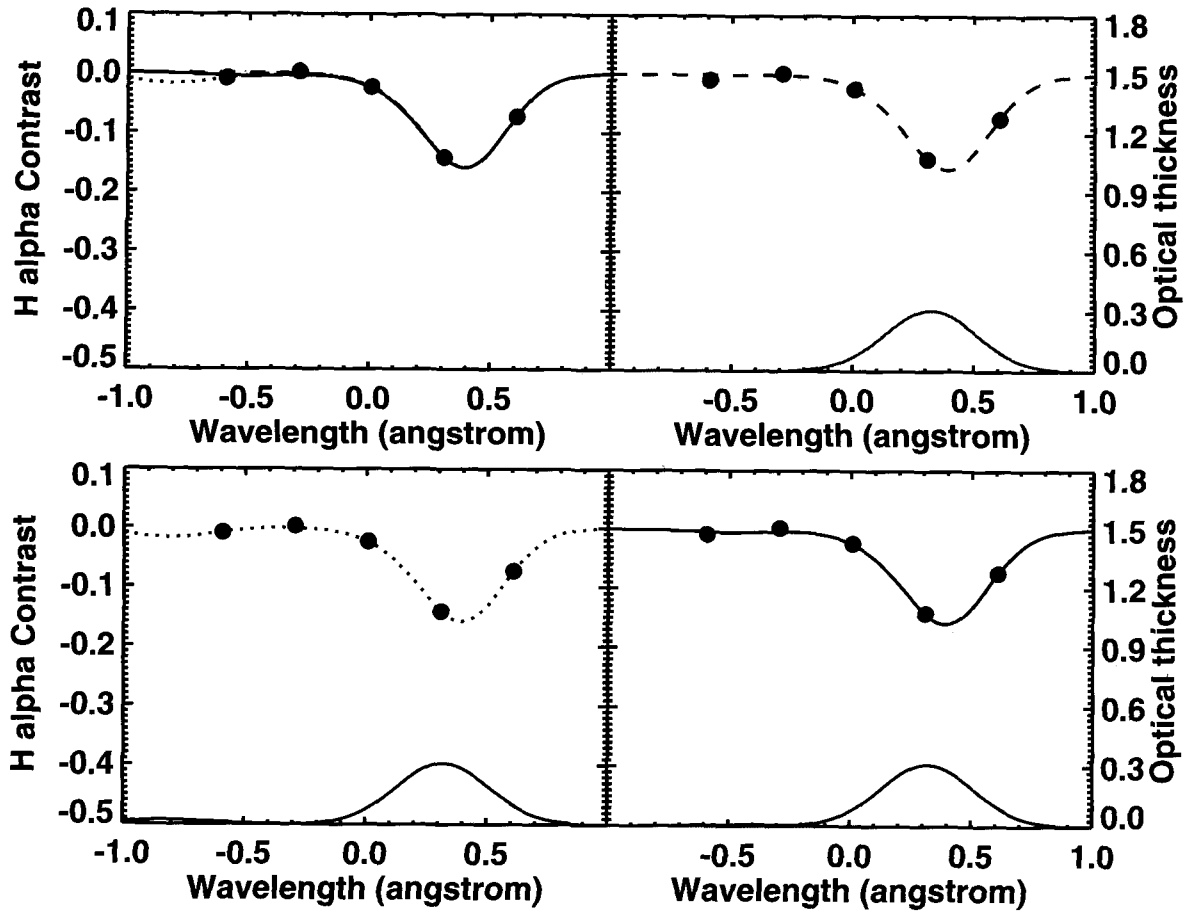

Fig. 3.— Spectral contrast profile at the point on a velocity thread, and the results of single-component, two-component , and three-component fits (from left to right, and from top to bottom). Each Gaussian curve refers to the optical thickness profile of the corresponding velocity component.

km s^{-1}, $v_b = -17.2$ km s^{-1}, $\tau_r = 0.51$, $\tau_s = 0.73$, and $\tau_b = 0.30$. Using these values, we may calculate a weighted average of the velocity over the three components as $\langle v \rangle \equiv (\tau_r v_r + \tau_b v_b)/(\tau_r + \tau_s + \tau_b) = 2.2$ km s^{-1}. This value is very close to the value $v_0 = 2.6$ km s^{-1} obtained from the single-component fit. The low value of the average velocity is attributed to the approximate symmetry between the blue-shifted and red-shifted components as well as the weight of the stationary component.

How many velocity threads contribute to the contrast data at this point? A simple way of getting an answer to this question is to divide the values of the optical thickness by 0.31, the value for a single resolved thread. We obtain 1.6, 2.3, and 0.97 as the numbers of threads in red-shifted, stationary, and blue-shifted components, respectively. Their sum is 4.9. The non-integer values can be understood either in terms of thread-to-thread variation of the single-thread optical thickness or in terms of a partial contribution of some threads to optical thickness. We can roughly say that the absorbing structure at this point consists of four or five threads.

(d) Spine

Similar results may be found from model fittings of the contrast data at a point inside the spine. The point marked by the symbol △ in Figure 2 represents the darkest region inside the spine. The color is slightly blueish, suggesting that it is a little blue-shifted.

The single-component model fit is not satisfactory for this contrast profile ($\chi^2 = 3.6$). Even worse is the two-component model fit ($\chi^2 = 15.7$). The three-component model fit is good enough ($\chi^2 = 0.01$). The line-of-sight velocities determined by the three-component fit are $v_r = +13.7$ km s^{-1} for the red-shifted component and $v_b = -17.2$ km s^{-1} for the blue-shifted component. The values of optical thickness are $\tau_r = 0.47$, $\tau_s = 1.51$, and $\tau_b = 0.78$, which

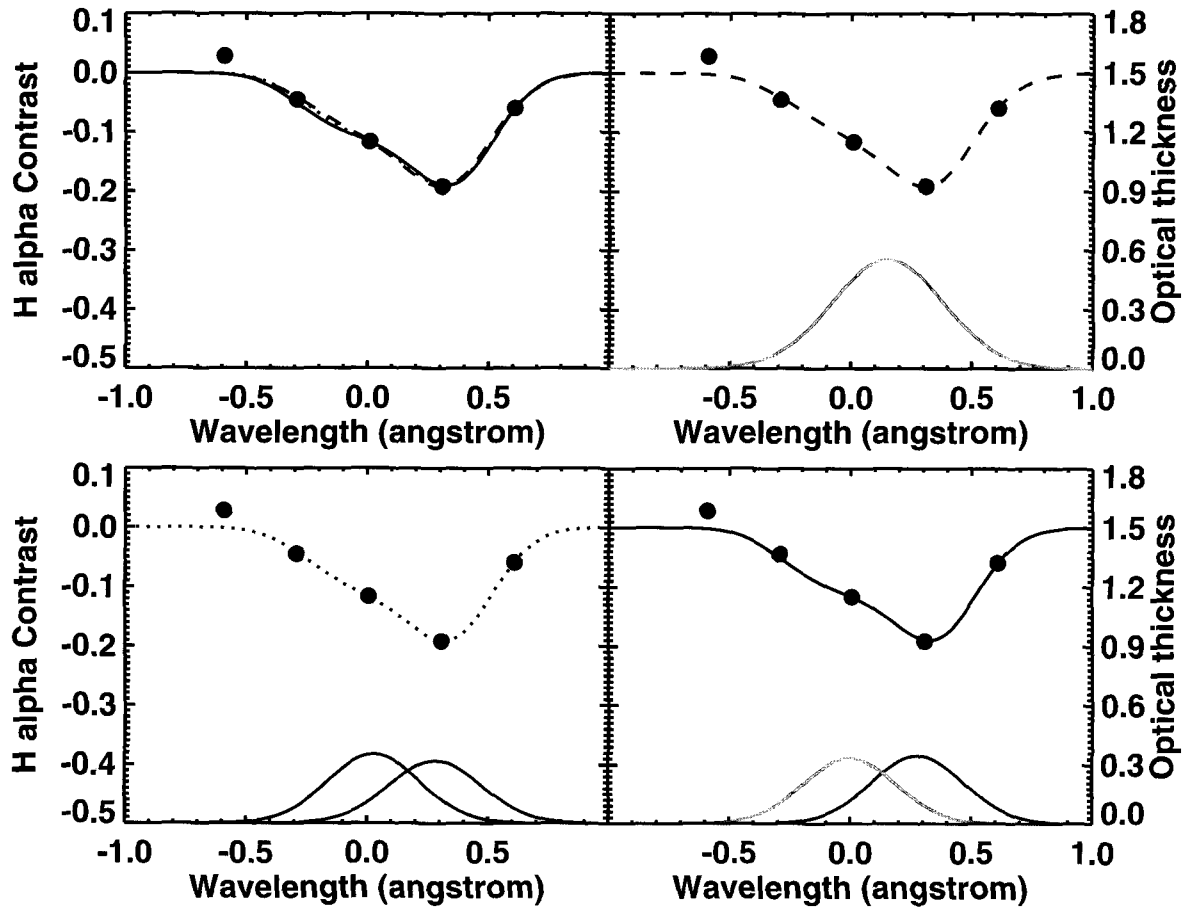

Fig. 4.— Contrast profile at the point (velocity thread 2), and the results of single-component, two-component, and three-component fits (from left to right, and from top to bottom).

correspond to 1.5, 4.9, and 2.5, respectively, for the number of threads. Their sum is 8.9. Recalling that this point represents the densest part of the filament, we find that the total number of threads at an arbitrary point inside the filament ranges from one to nine.

(e) Dependence on $\Delta\lambda_D$ and S/I_c

We have examined the dependence of line-of-sight velocities on the constraining simplifications in the three-component model. Note that S/I_c has been set to the value determined from the single-component fit. In this approach, the point-to-point variation of S/I_c is automatically taken into account. Its value is 0.10 at the barb point (∗), and 0.094 at the spine point (△). We have found that a slight change in S/I_c, say, by 5% affects the goodness of fit little, and results in a small variation in the line-of-sight velocity of less than 4%. The Doppler width $\Delta\lambda_D$ has been set to 0.27 Å. We have also found that a 10% variation in the Doppler width results in a variation in the line-of-sight velocities of less than 2%. Therefore it is concluded that the determination of the line-of-sight velocity using the three-velocity-component model is not very sensitive to the adopted values of $\Delta\lambda_D$ and S/I_c.

V. SPATIAL DISTRIBUTIONS OF MODEL PARAMETERS

(a) Single Component Model Parameters

Figure 7 shows the maps of Hα parameters determined from the single component cloud model fit of the set of 5 images taken at an instant (19:27 UT). The maps were constructed from the fitting of profiles at 240 × 160 spatial points, but the parameters at points outside the filament were suppressed in the figure for visibility. Note that the effect of the spectral contamination by fibrils is easily discernable from the $\Delta\lambda_D$ map, since such spectral contamination leads to very large values of $\Delta\lambda_D$. We avoid such contamination areas, and select two regions of interest (specified by two polygons in the figure) to represent the barb and the spine, respectively. The barb region consists of

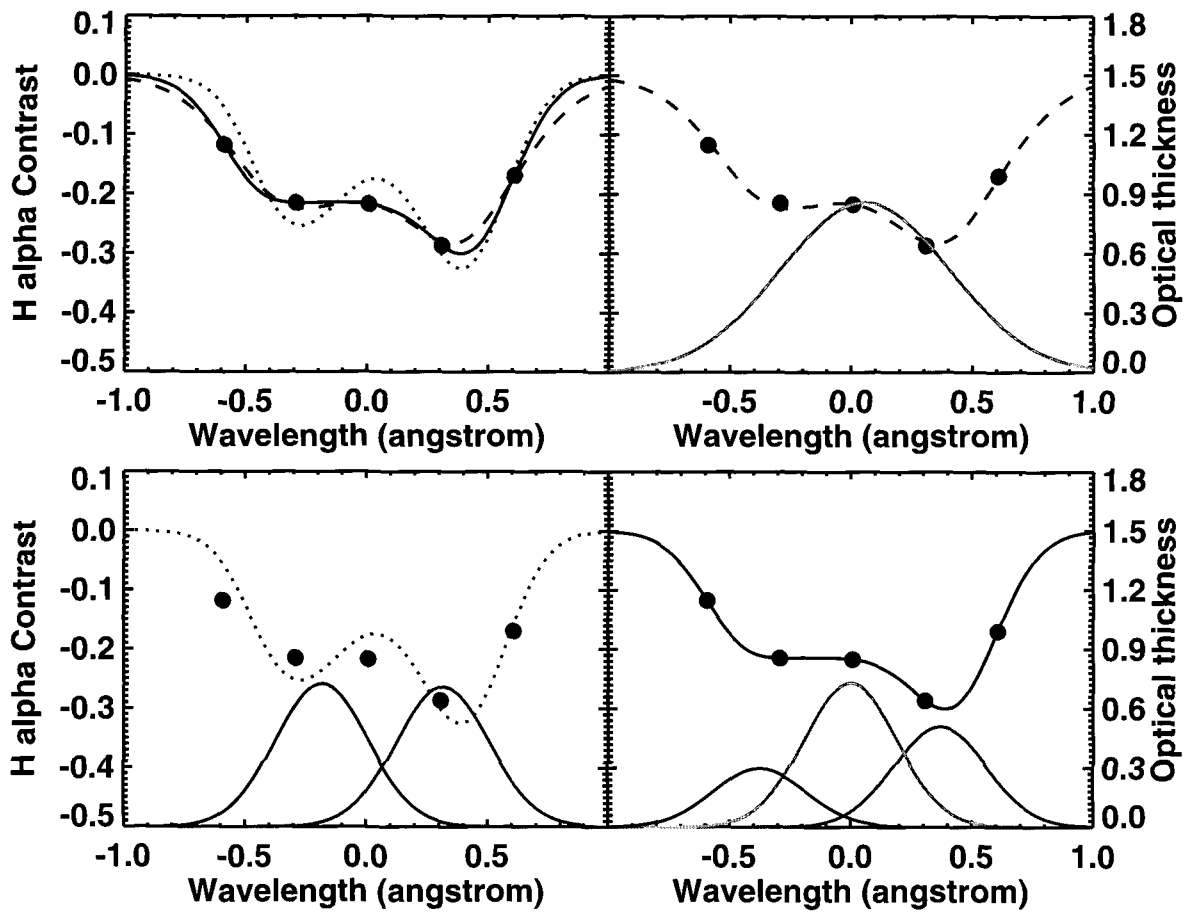

Fig. 5.— Spectral profile of contrast at a point inside the barb and the results of single-component, two-component, and three-component fits (from left to right, and from top to bottom).

1774 spatial points, and the spine region, of 1940 spatial points. The mean values and standard deviations of the parameters inside the spine and the barb are summarized in Table (b). These value are very comparable to those given in Paper I. As expected, Figure 7 and Table (b) indicate that the barb contains less Hα-absorbing material as measured by $\tau_0 \Delta\lambda_D$ than the spine, but is more dynamic than the spine as inferred from the larger mean of $\Delta\lambda_D$ and larger standard deviation of v_0.

Figure 7 clearly shows that the line-of-sight velocity structure of the barb is filamentary, often showing alternating signs side by side. This characteristic is another manifestation of the mixed existence of blueish threads and reddish threads in the color image, and may mean that plasma inside a thread moves independently of plasmas in neighboring threads, supporting the existence count-streaming flows previously reported by Zirker et al. (1998) and Lin et al. (2003).

In addition, a careful examination of the v_0 map reveals that the magnitude of v_0 tends to get much higher at spatial points near the edge than inside the filament. Note that the edge often has a velocity as high as 15 km s^{-1} while the magnitude of the velocity in the interior is usually lower than 10 km s^{-1}. This difference may be attributed to the number density of threads. In the interior of the filament, we may be observing several threads with different line-of-sight velocities that are overlapped along the line of sight. In this case, the cloud model fit may yield an average line-of-sight velocity that may be significantly lower than the velocities of individual threads. At the edge of the filament, such an overlapping effect may be less serious, resulting in less smearing and a higher line-of-sight velocity. This also explains the active features found at the edges of quiescent prominences by Engvold et al. (1978). If this is the case, line-of-sight velocities higher than 15 km s^{-1} may be common in threads in the interior as well as at the edge.

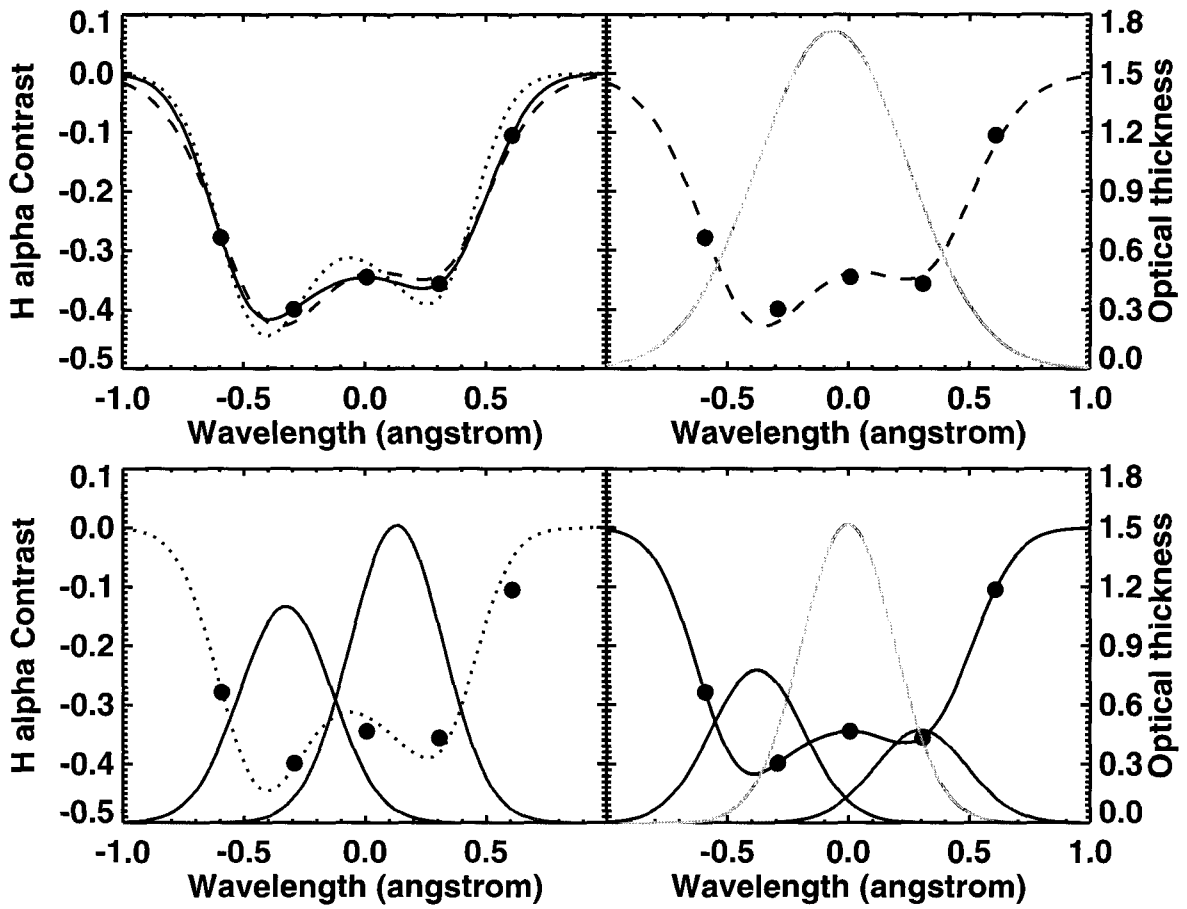

Fig. 6.— Spectral profile of contrast at a point inside the spine.

(b) Three-Component Model Parameters

Figure 8 presents maps of several parameters determined from three-component model fits. Prominent blue-shifted velocity threads are well discernable in the map of $\tau_b v_b$ and prominent red-shifted threads, in the $\tau_r v_r$ map. The visible portions of these prominent threads have lengths ranging from 10″ to 35″. This range partially overlaps the range of the lengths of thin threads, 5″ to 20″, reported by Lin et al. (2003).

Table (b) summarizes the results obtained from the three-component fit. Note that S/I_C at each spatial point was set to the value determined from the single-component fit and $\Delta\lambda_D$ to a constant value of 0.27Å. We have set a loose constraint on the fitting so that the two parameters v_b and v_r may have values not much different from -16 km s^{-1} and +16 km s^{-1}, respectively. The determined values have averages of -16 km s^{-1} and 15 km s^{-1} in the barb, and smaller values -14.6 km s^{-1} and 14 km s^{-1} in the spine.

In both the spine and the barb, blue-shifted components have slightly higher values of velocity and of optical thickness than red-shifted components, but the differences are very small. These small differences are consistent with non-zero average values of line-of-sight velocities obtained from the single component fit (see Table (b)). Except for these differences, we can say that there is a statistical balance between red-shifted components and blue-shifted components.

In the barb, we find that the sum of τ_b and τ_s for the moving components is the same as τ_s for the stationary components. This means that half of the filament material is moving at significant speeds while the other half is at rest. If we adopt 0.31 as the average optical thickness of a velocity thread, we can say that there are 1.3 blue-shifted velocity threads, 1.1 red-shifted threads, and 2.4 stationary threads on average along the line of sight at each spatial point. In the spine, a rough equality holds between $\tau_b + \tau_s$ and τ_s, too, but we find more threads than in the barb. We can say that there are 1.6 blue-shifted velocity threads, 1.5 red-shifted threads, and 3.6 stationary threads on average along the line of sight at each spatial point.

Summing up, on average each spatial resolution el-

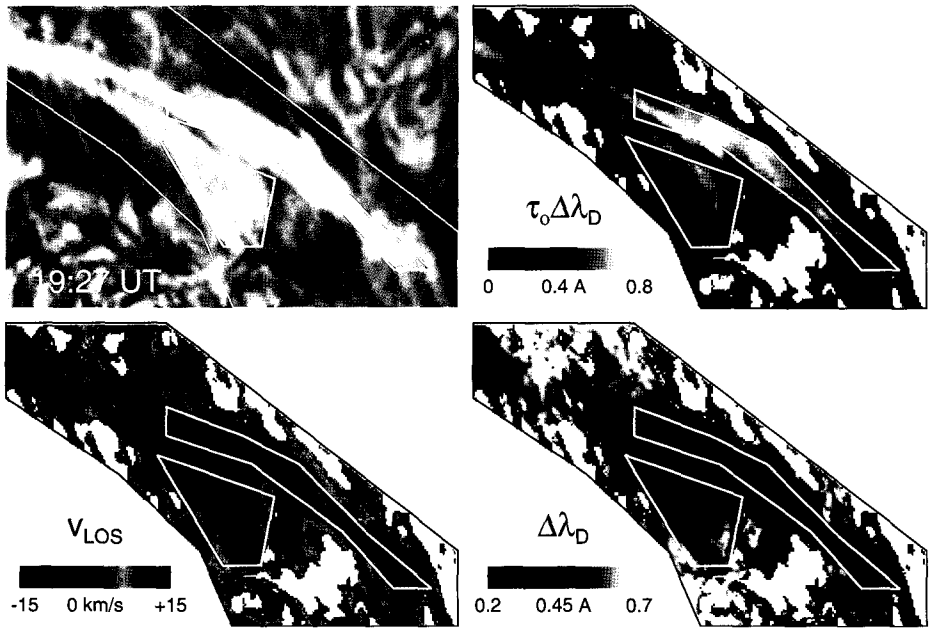

Fig. 7.— Color Hα image, and maps of Hα absorption parameters obtained from single-component model fits. The two polygons mark the areas of the barb and the spine that were used for statistics.

ement contains four threads inside the barb, and six threads in the spine. A quarter of those threads are moving toward us, another quarter are moving away from us, and the remaining half are at rest.

VI. TEMPORAL VARIATIONS OF MODEL PARAMETERS

Previous observations revealed the existence of oscillatory components with periods of a few minutes to half an hour as well as steady ones in the time variation of line-of-sight velocity in filaments (e.g., Lin et al 2003; Lin 2004). The amplitudes were found to be small (<2 km s^{-1}), which may be mainly because the line center method used by these authors seriously underestimates line-of-sight velocity in filaments (see the discussion in Paper I).

To examine the existence of similar oscillatory behaviors in our data, we have plotted the single-component model parameters and three-component model parameters in Figure 9 as functions of time during a period of about 100 minutes, at a fixed point inside the barb ($*$ symbol in Figure 2) and at another fixed point inside the spine ($\triangle$ symbol in Figure 2), respectively. The reference time in the plot is 19:27 UT. The model fits at this reference time are given in Figures 5 and 6.

The figures clearly show that the temporal variations of all the parameters consist of fluctuating components (standard deviations) as well as stationary components (means). Their temporal means and standard deviations are listed in Table VI.

In the case of single-component velocity, the fluctuating components dominate over the stationary components, especially in the barb. The velocity of the barb point was red-shifted at time zero, but in a couple of minutes it turned blue-shifted, implying that the velocity was oscillating. It is obvious, though, from the figure that the oscillation is not like a long train of well-defined sinusoids. The most pronounced sinusoid in the velocity plot inside the barb covers at most four cycles of about 5 minute period, and the one inside the spine covers only two cycles of about 12 minute period. The single component optical thickness also fluctuated in time, but its fluctuation is poorly correlated with that of line-of-sight velocity.

Temporal fluctuation is also obvious in the time variations of parameters determined from the three component model fits. The comparison between the means and standard deviations of these parameters given in Table VI indicates that the stationary components (means) dominate over the fluctuating components (standard deviations), in contrast to the results of the single-component model fits.

Figure 10 shows that the difference between τ_r and τ_b is strongly correlated with the single-component velocity v_0. The correlation coefficient is found to be 0.85. This means that when τ_b exceeds τ_r, the single-component velocity is usually blue-shifted, and when τ_r exceeds τ_b, it is usually red-shifted. Not only the non-zero value of velocity in the single-component model is explained by the small difference between τ_b and τ_r, but also its oscillatory behavior can be attributed to the temporal variation of $\tau_r - \tau_b$. This gives us a lesson that one should be very careful in interpreting the line-of-sight velocities inferred from the single-component model fit as well as their oscillatory behaviors.

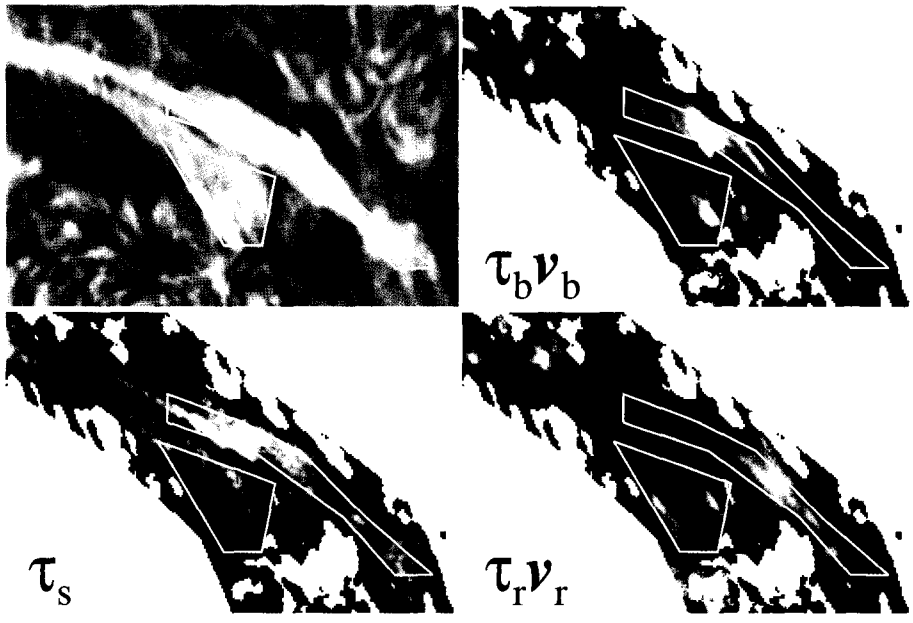

Fig. 8.— Color Hα image and maps of $\tau_b v_b$ for the blue-shifted component, τ_s for the stationary component, and $\tau_r v_r$ for the red-shifted component.

VII. SUMMARY AND DISCUSSION

(a) Summary

From the analysis of the Hα image data of a filament taken at different wavelengths, we have confirmed that a filament consists of numerous velocity threads. A well-resolved velocity thread was characterized by a narrow Doppler width $\Delta\lambda_D = 0.27$ Å and a small optical thickness $\tau_0 = 0.31$. The values of $\Delta\lambda_D$ and τ_0 determined from single-component model fits at a point inside the filament were usually much bigger than these values, which supports the view that more than one velocity thread contributes to the data. It has been inferred that usually four to six threads lie along the line of sight at each spatial resolution element.

We have obtained results supporting the view that plasma in some threads comprising the filament moves fast with a line-of-sight speed of about 15 km s^{-1}. The first piece of evidence is our identification of a spatially and spectrally well-resolved velocity thread, having a line-of-sight speed of 14.6 km s^{-1}. Its spectral data were so well fitted by the single-component model with a narrow Doppler width (Figure 3) that there is no ambiguity in interpreting the result at all. In addition, it was found from the line-of-sight velocity map constructed from single-component model fits (Figure 7) that many spatial resolution elements at the edge of the filament have line-of-sight speeds as high as 15 km s^{-1}. The prevalence of fast-moving threads inside the filaments has also been supported by the result of three-component model fits. On average the spectral data inside the filament are best explained by introducing high velocity components with velocities in the range 14 to 18 km s^{-1}.

Suppose the major direction of velocity vectors of motion whose line-of-sight components we observe is horizontal. Then our results suggest that plasma in the many threads comprising the filament moves horizontally as fast as 30 km s^{-1}, since the magnitude of horizontal velocity vectors should be bigger than $v_{LOS}/\sin\theta$, where θ is the heliocentric angle between the disk center and the observed region. In our observations we have $\cos\theta = 0.87$ and hence $\sin\theta = 0.49$, and the average line-of-sight speed v_{LOS} was equal to 15 km s^{-1}.

Our results from three-component fits also support the view that a significant fraction of the material comprising the filament is at rest. Of course, this may not necessarily mean that all the plasma constituting the stationary component is totally at rest. We will discuss this aspect in the following.

(b) Velocity distribution of threads

Inferring line-of-sight velocities of threads from the data is an inversion problem whose solution may not be unique. Therefore there could be an objection to our interpretation for a *trimodal* velocity distribution that plasma in threads either is at rest or moves bidirectionally at fast speeds.

Firstly, we raise a question whether the existence of the stationary component is required to explain the

TABLE 2.
MEAN VALUES AND STANDARD DEVIATIONS OF MODEL PARAMETERS INSIDE THE BARB AND SPINE, RESPECTIVELY. THE BARB REGION CONSISTS OF 1774 SPATIAL POINTS, AND THE SPINE REGION, OF 1940 SPATIAL POINTS.

	Parameter	Barb	Spine
Single-comp. model	S/I_c	0.10± 0.015	0.094±0.007
	$\Delta\lambda_D$	0.47±0.08 Å	0.42±0.04 Å
	τ_0	0.88±0.26	1.35±0.32
	$\tau_0\Delta\lambda_D$	0.40±0.09 Å	0.56±0.13 Å
	v_0	-0.8±4.0 km s^{-1}	-0.2±1.8 km s^{-1}
Three-comp. model	$\Delta\lambda_D$	0.27 Å	0.27 Å
	v_b	-16.0 ± 2.3 km s^{-1}	-14.6 ± 1.9 km s^{-1}
	v_r	$+15.0 \pm 2.9$ km s^{-1}	$+14.0 \pm 2.3$ km s^{-1}
	τ_b	0.40 ± 0.11	0.49 ± 0.14
	τ_s	0.74 ± 0.23	1.12 ± 0.28
	τ_r	0.34 ± 0.12	0.46 ± 0.11

TABLE 3.
MEAN VALUES AND STANDARD DEVIATIONS OF THE TEMPORAL VARIATIONS OF SINGLE-COMPONENT MODEL PARAMETERS AND THREE-COMPONENT MODEL PARAMETERS AT A FIXED POINT INSIDE THE BARB AND AT ANOTHER FIXED POINT INSIDE THE SPINE, RESPECTIVELY.

	Parameter	Barb	Spine
Single comp. model	v_0	-1.4±3.1 km s^{-1}	-1.6±1.3 km s^{-1}
	τ_0	0.59±0.18	1.6±0.20
Three comp. model	v_b	-17.6±1.5 km s^{-1}	-16.1±1.1 km s^{-1}
	v_r	16.7±2.9 km s^{-1}	13.9±1.7 km s^{-1}
	τ_b	0.31 ± 0.07	0.66±0.07
	τ_s	0.50 ± 0.16	1.40 ± 0.21
	τ_r	0.27 ± 0.11	0.53±0.07

data. Our answer is yes. Looking at the data shown in Figure 6 reveals that the two-component model without the stationary component does not fit the data well whereas the single-component model and the three-component model allowing the stationary component fit the data quite well. Moreover, in the three-component model, the optical thickness of the stationary component is bigger than those of the two moving components, which indicates that the existence of the stationary component is crucial.

Secondly, does the goodness-of-fit of the models with the stationary component mean that the velocity of all the plasma constituting the stationary component is literally zero? It may not necessarily be so, for the stationary component in fact may consist of a number of threads that have different velocities, either negative or positive. It is likely that the velocities of threads contributing to the stationary component are distributed around zero, ranging from a negative value to a positive value, so the average of thread velocities may be close to zero, but their standard deviation may not.

From our results, it is possible to estimate this velocity deviation of threads that would appear as stationary components in our three-component analysis. Note fast moving threads are not included in this consideration. Suppose each of the individual threads has the same Doppler broadening factor $\sigma_{D,th}$ in velocity units of km s^{-1}. Then the standard deviation of thread velocities σ_v is related to the standard deviation of the absorption profile of the stationary component σ_S (in velocity units) through

$$\sigma_v^2 + \sigma_{D,th}^2 = \sigma_S^2 . \quad (8)$$

Since our three-component model adopted $\Delta\lambda_D = 0.27$ Å for the stationary component, it follows $\sigma_S = 45\Delta\lambda_D/\sqrt{2} = 8.6$ km s^{-1}. Another critical factor in the determination of σ_v is $\sigma_{D,th} = 45\Delta\lambda_{D,th}/\sqrt{2}$ of the individual threads. The Doppler broadening $\Delta\lambda_{D,th}$ is determined by the temperature and micro-turbulence inside each of the individual threads. If we choose the average values $T = 6400$K and $\xi = 5.5$ km s^{-1} given in Table 3.4 of Tandberg-Hanssen (1995), we get $\sigma_{D,th} = 8.0$ km s^{-1} and $\sigma_v = 3.2$ km s^{-1}. The nature of micro-turbulence is not still known. If we assume the extreme situation that the mysterious micro-turbulence is also wholly attributed to unresolved velocity threads, then we obtain a higher value of velocity dispersion $\sigma_v = 6.3$ km s^{-1}.

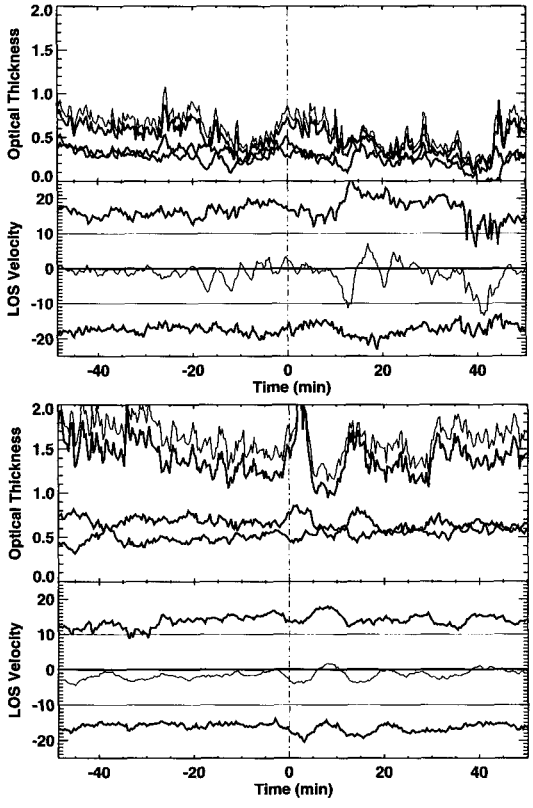

Fig. 9.— Time variations of cloud model parameters at a point inside the barb (left) and at a point inside the spine (right). The black color refers to the parameters of the single-component fit, and the red, green, and blue colors refer to those of the red-shifted component, the stationary component, and the blue-shifted component, respectively.

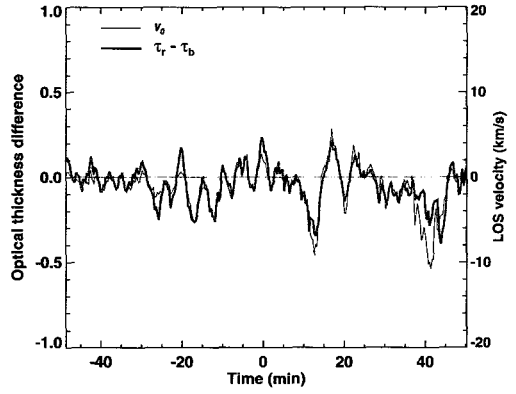

Fig. 10.— Time variations of $\tau_r - \tau_b$ obtained from three-component model fits and v_0 obtained from single-component model fits at the barb point.

Another way to infer the velocity dispersion of the stationary component is to make use of the velocity dispersions obtained from the moving components. Note in our three-component model the velocity of the stationary component is fixed to zero for the purpose of limiting the number of free parameters while those of the two moving components are treated as free parameters to be determined from data. It is expected that the velocity dispersion of the stationary component is close to those of the other components. According to Table 2, the real velocity dispersion of the blue-shifted component is 1.9 and 2.3 km s^{-1}, and that of the red-shifted component is 2.3 and 2.9 km s^{-1}, depending on the region of the filament. We find that the biggest value 2.9 km s^{-1} is comparable to the smaller value 3.2 km s^{-1} obtained above. Based on these estimates we may regard the stationary component as a superposition of slowly moving threads whose line-of-sight velocity is distributed around zero with a standard deviation that is less than 6 km s^{-1}, probably around 3 km s^{-1}.

Finally, we discuss whether the velocity distribution of threads is continuous or discrete. If threads are numerous enough and have different velocities, the velocity distribution may appear continuous. On the other hand, if the number of threads is small, the velocity distribution may be discrete. If the width of the velocity components is narrow enough, different velocity components may appear as a finite number of peaks (or valleys) in the spectral data. Unfortunately, $\Delta\lambda_D$ of the Hα line is too big to be used for this purpose. Instead, the Ca II K line can be used for it since it has a smaller value. The spectral observations of quiescent prominences reported by Engvold et al. (1978) provided such evidence. They provided in their Fig. 5 some nice examples of line profiles where a finite number of velocity components are spectrally well resolved in the Ca II K lines having a smaller $\Delta\lambda_D$ even though they are not obvious in Hα line profiles with a bigger $\Delta\lambda_D$. This observation suggests that velocity distribution inside a filament/prominence may be discrete rather being continuous.

(c) Comparison with Previous Observations

One of the main results of our study is that in a significant fraction of threads constituting the filament, plasma moves fast with line-of-sight speeds of 15 km s^{-1}. Note that the filament we studied was quiescent, neither erupting nor activating, even if it was undergoing continual change as most quiescent filaments do.

Table (b) lists the values reported from previous studies. Our results look much different from previous observations. However this apparent discrepancy does not necessarily mean the real difference since the measured line-of-sight velocities may depend on various factors such as the method of analysis, the orientation of line of sight, the filament activity, the specific parts of filaments that are analyzed, and whether threads are resolved or not. Carefully taking these factors into account, we find that in a broad sense our results are consistent with previous observations.

TABLE 4.
LINE-OF-SIGHT VELOCITY MEASUREMENTS FROM Hα OBSERVATIONS OF FILAMENTS/PROMINENCES. IN THE LAST COLUMN, THE NUMERICS INSIDE THE BRACKETS REPRESENT THE LOWER AND UPPER BOUNDS, AND THE BOLD-FACED NUMERICS REFER TO THE AVERAGE OR TYPICAL VALUES. THE OTHER NUMERICS ARE SOME SPECIFIC EXAMPLES. (AR: ACTIVE REGION FILAMENT, QS: QUIESCENT FILAMENT/PROMINENCE, PC: POLAR CROWN FILAMENT)

Paper	Method	Objects	Location	Values (km s^{-1})
Mein (1977)	±0.45 Å chord	AR		[-6, 6]
Martres et al. (1981)	±0.27 Å chord	QS	(N17, E25)	[-7,7]
Malherbe et al. (1981)	±0.30 Å chord	QS	(N36, W20)	[-3, 3]
Kubota & Uesugi (1986)	Line minimum	QS	(S6, E10)	[-6, 6]
You & Engvold (1989)	Bisector	QS	$\cos\theta = 0.94$	[-1.7, 2.7]
Simon et al. (1986)	±0.30 Å chord	QS	(S20, W34)	[-3, 3]
Schmieder et al. (1991)	±0.256 Å cord	QS	(N5, W5)	[-2.5, 2.5]
Schmieder et al. (1991)	differential cloud model	QS: footpoints	(N5, W5)	-17, 14, 17
Lin et al. (2003)	Line center	PC	(S47, E27)	[-3, 3]
Engvold et al. (1978)	Line center	QS: edge	Limb	**34**
Mein et al. (1989)	Line center	QS	Limb	[-15, 15]
Kulidzanishvili (1989)	Line center	QS	Limb	[-4, 30]
Present study	Single-comp. cloud model	QS: spine	(N15, E26)	[-5, 5]
Present study	Single-comp. cloud model	QS: barb	(N15, E26)	[-13, 13]
Present study	Single-comp. cloud model	QS: thread	(N15, E26)	15
Present study	Three-comp. cloud model	QS: threads	(N15, E26)	**-15, 0, 15**

It can be inferred from Table (b) that observations performed near the disk center (You & Engvold 1989; Schmieder et al. 1991) presented the smallest values of line-of-sight velocity, while the limb observations (Engvold et al. 1978, Mein et al. 1989, Kulidzanishvili 1989) gave the biggest values. This kind of difference may be attributed to the difference in the orientation of the line of sight, and supports the view that the predominant direction of motion in filaments/prominences is horizontal.

The method of analysis used is also partly responsible for the apparent discrepancy. Lin et al. (2003) used the line-center method which yielded very small values of line-of-sight velocity in a filament that was far away from the disk center. Note the center of the Hα profile in disk observations is affected much more by the underlying photosphere and chromosphere than by the filament. The line-of-sight velocities determined with this method are always underestimated as we discussed in Paper I. This method, however, finely works in prominence observations off the limb where background radiation is negligible. The chord method for disk observations is subject to the same problem, even if it seems to be less affected by the underlying atmosphere than the line-center method. On the contrary, the line-of-sight velocity determined by applying the cloud model fit is little affected by the underlying atmosphere, and reflects fairly well the velocity of filaments. The velocity range determined using the single-component fit in our study is from -13 to 13 km s^{-1}, much bigger than the range from -7 to 7 km s^{-1}, the biggest values reported from disk observations using the chord method. Interestingly the values we obtained are comparable to the values obtained by Schmieder et al. (1991) who used a similar method (differential cloud model), and the values obtained by Mein et al. (1989) from limb observations.

Finally we emphasize that whether threads are resolved or not is another important factor in understanding the difference in the values of line-of-sight velocity. Our study indicates that threads that are either spatially or spectrally resolved have higher line-of-sight velocities than unresolved threads. Note that threads are spatially resolved well in the order of edges, barbs, spines. The line-of-sight value reported by Engvold et al. (1978) is the highest ever reported in previous observations. We think that it represents a typical moving thread that often exists inside filaments. The main reason the velocity is so high may be that it reflects the line-of-sight velocities of threads that are well resolved both spatially and spectrally. It may not be a simple coincidence that the typical horizontal velocity of 30 km s^{-1} we obtained in the present study is close to the value 34 km s^{-1} Engvold et al. (1978) reported.

(d) A Picture of Filament Fine Structure

A new picture of filament fine structure emerges from our study. As Figure 11 illustrates, a part of a filament is composed of fine velocity threads that are either stationary (or moving slowly) or moving at high speeds. In our observations, each spatial resolution element contains about four to six threads along the line of sight. In about half of the threads, plasma moves horizontally, probably along threads, at high speeds of about 30 km s^{-1}, while in the other half of the threads plasma is either at rest or moving slowly. In half of the moving threads, plasma moves in one direction and in the other half of the moving threads, plasma moves in the opposite direction.

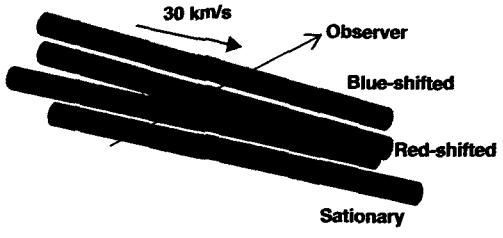

Fig. 11.— Picture of the filament fine structure that consists of stationary velocity threads and fast-moving velocity threads.

This picture is well supported by recent observations of plane-of-sky motions in quiescent filaments and prominences. Based on off-band Hα observations of filaments located far away from the disk center, Zirker et al. (1998) first reported the simultaneous existence of oppositely directed flows in adjacent threads — the counter-streaming flows. The speeds were in the range 5 – 20 km s^{-1}. Lin et al. (2003) reported speeds of about 8 km s^{-1} in a polar crown filament. Later Lin et al. (2006) presented even bigger values of about 15 km s^{-1}. Note that the spatial resolution was the highest in the observations of Lin et al. (2006), supporting the view that it is very crucial to resolve individual threads as we mentioned above. The last value is comparable to the value we obtained for the line-of-sight velocity of fast-moving plasma using the three-component cloud model. If the geometric projection effect is taken into account, with the assumption that plasma motion is mainly horizontal, the horizontal velocity would turn out to be much bigger than this value, and there is enough room for 30 km s^{-1}. It is very interesting that the typical horizontal speed inferred from He IIλ304 observations of prominences on the limb was 30 km s^{-1} (Wang 1999), even if higher velocities up to 70 km s^{-1} were not rare in UV/EUV observations (Kucera et al. 2003).

Our results on the number of threads (4–6) are highly consistent with the results of previous studies (Engvold et al. 1989; Mein & Mein 1991; Mein et al. 1994). Engvold et al. (1989) examined the line intensity and line width versus the line-of-sight velocity. The line width was the narrowest for a line-of-sight velocity of about 20 km s^{-1}. So they regarded the average intensity at such velocities as the typical intensity of individual threads and concluded that spatial resolution elements with low line shifts contain 3–5 threads. Mein & Mein (1991) analyzed the distribution of line width and line-of-sight at each beam of intensity in the unresolved features of a quiescent prominence. They assumed that the elementary threads have an optical thickness of 0.2 and a temperature of 8500 K, and produced statistical models that best match the observed dependence of the means and standard deviations of line width and the standard deviation of line-of-sight velocity. As a result, they found that there are 6 threads with a line-of-sight velocity dispersion of about 7 km s^{-1} in the spatial resolution element inside the central parts of the prominence. A similar method was applied to a quiescent filament by Mein et al. (1994). It was found that most spatial resolution elements were composed of 2–4 threads that have a velocity dispersion of 3.5 km s^{-1} if the optical thickness of each thread is 0.2.

VIII. CONCLUSION

We have obtained results supporting the view that some plasma constituting a quiescent filament moves fast, being consistent with recent high resolution observations from ground and EUV observations from space. At the same time our results also indicate that a significant fraction of plasma constituting the same feature is at rest or moving slowly. Therefore the existence of high speed flows in filaments/prominences can not completely negate the need for magnetic dips that should sustain cool stationary or low-speed plasma against gravity.

From our results we also have learned an important lesson that decomposing threads spectrally and spatially is crucial for interpreting the physical nature of motions, either flows or oscillations, observed in filaments/prominences. Spatially resolving threads requires a spatial resolution as high as a few tenths of an arc second, which has been achieved in a very limited number of observations (e.g., Lin et al. 2005). The forthcoming observations to be performed either in space or on the ground are aimed to achieve such high spatial resolution, so we will get a much better opportunity to study spatially resolved threads. Nevertheless it should be kept in mind that threads overlapped along the same line-of-sight can not be resolved even with this kind of very high spatial resolution only. Our study demonstrates that spectrally resolving threads is also required to separate threads having different line-of-sight velocities. An ideal way is to combine both approaches, resolving spatially and spectrally. This requires imaging spectroscopy with very high spatial resolution.

ACKNOWLEDGEMENTS

The constructive comments of the referee are much appreciated. This work was supported by the Korea Research Foundation Grant funded by the Korean Government(KRF-2005-070-C00059).

REFERENCES

Chae, J., Yun, H. S., & Poland, A. I. 1998, Temperature Dependence of Ultraviolet Line Average Doppler Shifts in the Quiet Sun, ApJS, 114, 151

Chae, J., Denker, C., Spirock, T. J., Wang, H., & Goode, P. R. 2000, High-Resolution H_α Observations of Proper

Motion in NOAA 8668: Evidence for Filament Mass Injection by Chromospheric Reconnection, Sol. Phys., 195, 333

Chae, J. 2003, The Formation of a Prominence in NOAA Active Region 8668. II. Trace Observations of Jets and Eruptions Associated with Canceling Magnetic Features, ApJ, 584, 1084

Chae, J., Moon, Y.-J., & Park, Y.-D. 2005, The Magnetic Structure of Filament Barbs, ApJ, 626, 574

Chae, J., Park, Y.-D., & Park, H.-M. 2006, Imaging Spectroscopy of a Solar Filament Using a Tunable H_α Filter, Sol. Phys., 234, 115 (Paper I)

Engvold, O. 1976, The fine structure of prominences. I - Observations - H-alpha filtergrams, Sol. Phys., 49, 283

Engvold, O., Malville, J. M., & Livingston, W. 1978, The fine structure of prominences. V - Active edges of quiescent prominences, Sol. Phys., 60, 57

Engvold, O., Jensen, E., Zhang, Y., & Brynildsen, N. 1989, Distribution of velocities in the Pre-Eruptive Phase of a Quiscent Prominence, Hvar Observatory Bulletin, 13, 205

Karpen, J. T., Antiochos, S. K., & Klimchuk, J. A. 2006, The Origin of High-Speed Motions and Threads in Prominences, ApJ, 637, 531

Kubota, J., & Uesugi, A. 1986, The vertical motion of matter in a prominence observed on May 7, 1984, PASJ, 38, 903

Kucera, T. A., Tovar, M., & de Pontieu, B. 2003, Prominence Motions Observed at High Cadences in Temperatures from 10,000 to 250,000 K, Sol. Phys., 212, 81

Kucera, T. A., & Landi, E. 2006, Ultraviolet Observations of Prominence Activation and Cool Loop Dynamics, ApJ, 645, 1525

Kulidzanishvili, V. I. 1989, Mass Motions in a Quiescent Prominence and an Active One, Hvar Observatory Bulletin, 13, 215

Lin, Y., Engvold, O. R., & Wiik, J. E. 2003, Counterstreaming in a Large Polar Crown Filament, Sol. Phys., 216, 109

Lin, Y., 2004, Ph. D thesis, University of Oslo

Lin, Y., Engvold, O., Rouppe van der Voort, L., Wiik, J. E., & Berger, T. E. 2005, Thin Threads of Solar Filaments, Sol. Phys., 226, 239

Malherbe, J. M., Schmieder, B., & Mein, P. 1981,Dynamics in the filaments. I - Oscillations in a quiescent filament, A&A, 102, 124

Martres, M.-J., Mein, P., Schmieder, B., & Soru-Escaut, I. 1981, Structure and evolution of velocities in quiescent filaments, Sol. Phys., 69, 301

Mein, P. 1977, Multi-channel subtractive spectrograph and filament observations, solphys, 54, 45

Mein, P. 1994, Fine Structure of Prominences and Filaments, IAU Colloq. 144: Solar Coronal Structures, 289

Mein, P., & Mein, N. 1991, Dynamical fine structure of a quiescent prominence, Sol. Phys., 136, 317

Mein, P., Mein, N., Schmieder, B., & Noens, J. C. 1989, Dynamical Structure of a Quiescent Prominence, Hvar Observatory Bulletin, 13, 113

Mein, N., Mein, P., & Wiik, J. E. 1994, Dynamical fine structure of a quiescent filament, Sol. Phys., 151, 75

Mein, N., Schmieder, B., DeLuca, E. E., Heinzel, P., Mein, P., Malherbe, J. M., & Staiger, J. 2001, A Study of Hydrogen Density in Emerging Flux Loops from a Coordinated Transition Region and Coronal Explorer and Canary Islands Observation Campaign, ApJ, 556, 438

Schmieder, B., Raadu, M. A., & Wiik, J. E. 1991, Fine structure of solar filaments. II - Dynamics of threads and footpoints, A&A, 252, 353

Simon, G., Schmieder, B., Demoulin, P., & Poland, A. I. 1986, Dynamics of solar filaments. VI - Center-to-limb study of H-alpha and C IV velocities in a quiescent filament, A&A, 166, 319

Wallace, L., Hinkle, K., & Livingston, W. 1998, An atlas of the spectrum of the solar photosphere from 13,500 to 28,000 cm-1 (3570 to 7405 A), Publisher: Tucson, AZ: National Optical Astronomy Observatories, 1998

Wang, Y.-M. 1999, The Jetlike Nature of HE II lambda304 Prominences, ApJ, 520, L71

You, J.-Y. & Engvold, O. 1989, Vertical Flows in a Quiescent Filament, Hvar Observatory Bulletin, 13, 197

Zirker, J. B., & Koutchmy, S. 1990, Prominence fine structure, Sol. Phys., 127, 109

Zirker, J. B., & Koutchmy, S. 1991, Prominence fine structure. II - Diagnostics, Sol. Phys., 131, 107

Zirker, J. B., Engvold, O., & Martin, S. F. 1998, Counterstreaming gas flows in solar prominences as evidence for vertical magnetic fields, Nature, 396, 440